ORIGINAL PAPER

Study on overlying strata movement patterns and mechanisms in super-large mining height stopes

Jicheng Zhang[1] · Xuelong Li[1] · Qizhi Qin[1,2] · Yabo Wang[1] · Xin Gao[1]

Abstract

Aiming at the problem of strong mining pressure in the near shallow buried and super-large mining height face, and considering the first 108 working faces in Jinjitan Coal Mine as the engineering background, the movement pattern and pressure distribution characteristics of the overlying rock layer on the 8.2 m fully mechanized mining face were analyzed from the perspective of theoretical analysis, field monitoring data, and numerical simulation. The results of the spatial structure mechanics model and FLAC^{3D} numerical model of the mining face with a super-large mining height established in this study, which indicated that the mining operation of the mining face with a super-large mining height experienced rock dynamic load pressure and large-small periodic pressure phenomena. The fracture of the lower keystone beam leads to a small pressure cycle, and a large pressure cycle occurs when both the upper and lower keystone beams are fractured. Generally, the step distance during the size cycle is about twice the normal cycle. The site monitoring data shows that the initial incoming pressure step is 102 m and the periodic incoming pressure step is about 28.7 m, which is consistent with the theoretical value. When the working surface advances slowly, the dynamic load factor is smaller, and the incoming pressure step and duration are shorter, and vice versa. The research results are of important reference significance for mine pressure law and disaster prevention in similar conditions.

Keywords Super-large mining height · Near shallow coal seam · Rock movement · Rock pressure behavior · Periodic weighting

Introduction

As the energy crisis continues to intensify, the basic industrial status of coal as the main source of energy has not changed because it is still considered the main energy source in the future (Le et al. 2017; Hao et al. 2017). Thick coal seams and extra-thick coal seams occupy an important share in coal resource mining, and thick coal seam mining technology is the focus of coal mining technology, whose mining effect and quality will directly affect the development of the coal industry and energy security level (Yu et al. 2015). Usually, the technique of mining thick coal seam at the full height at one time is adopted, but the large mining height working face is prone to problems such as coal wall spalling

and poor stability of end face roof and support (Yuan et al. 2013; Wu et al. 2020; Li et al. 2017). Furthermore, when the lower coal seam is mined, the initial pressure of the top plate is more intense and the dynamic pressure phenomenon is more obvious. This seriously affects the mining efficiency and potential of the large mining face (Lu et al. 2022; Guo and Yang 2021). Therefore, how to mine thick coal seams safely and efficiently is an important issue in the coal industry worldwide (Li et al. 2020a, b, 2021a).

Benefiting from the progress of mining theory, technology, and equipment manufacturing, large mining height mining technology has been rapidly developed in recent years (Li et al. 2021a, b; Liu et al. 2019; Bai et al. 2019). When the mining height gradually grows 5–8 m or higher, the fissures become more developed, resulting in frequent rock activity within the fissure zone (Chen et al. 2022). Moreover, the roof thickness increases with the increase in mining height, and the key layer of the top plate has a more significant influence on the overlying lithology of the quarry. Thus, the traditional theory of controlling the quarry envelope will not be able to guide the coal mining activities under the

✉ Xuelong Li
   lilxcumt@126.com

1 State Key Laboratory of Mining Disaster Prevention and Control, Shandong University of Science and Technology, Qingdao 266590, China

2 Yankuang Group Co. LTD, Jining 272100, China

conditions of large or very large mining heights (Zhu et al. 2014). The researchers deduced a theoretical model applicable to large mining heights under limited conditions by analyzing field measurement data (Li et al. 2019a, b; Yan et al. 2020). Wen et al. (2019) proposed a method to determine the working load and yield of the support under the conditions of "given deformation" and "limited deformation" to put forward the roof control design and support selection calculations for the stope with a large mining height. Cheng et al. (2017) believed that the sub-key layer of a mining face with an extremely large mining height is easy to enter the collapse zone; thus, it cannot form a stable "masonry beam" structure like a normal working face, and the "cantilever beam" structure is periodically broken. Several researchers have validated the theoretical model of oversized extraction height by simulating experiments with similar materials. Shi and Zhang (2021) obtained the influence of mining height on the overburden collapse characteristics by comparing the overburden damage data measured in the field with the results of similar material simulation experiments. Then they optimized the prediction formula of the influence law of mining height on the height of the hydraulic conductivity fracture zone. Wu et al. (2016) evaluated the structural rupture mode of the roof slab in a large mining face and proposed a reasonable support resistance determination method through similar material simulation and theoretical analysis. They modified the traditional method of calculating the roof slab collapse height and put forward the method of determining the length and height of each structural area of the roof slab. Numerical simulation is a useful complement to oversized mining conditions. Li et al. (2019a, b) classified the movement types of the first critical layer into six types by theoretical analysis and numerical simulation, and then they determined the resistance of the support at the large mining face according to the movement types. They also established a load calculation model for each movement type and verified the accuracy of the model by comparing it with several actual field-measured data. Unver and Yasitli (2006) simulated the collapse mechanism of thick coal seams at long-arm working faces through FLAC^{3D} and established a top coal fracture-collapse prediction model. A special prefracture blasting strategy just sufficient to form cracks in the top coal is suggested by comparing physical results with those of numerical modeling.

The above investigations provide a good research basis and direction for the overlying rock movement law in large mining height conditions, but the current research findings are poorly generalized and are different greatly from the actual field-measured data (He et al. 2021). Based on the measured overburden activity in the far field and rock pressure in the near field of the first mining face of the Jinjiitan coal mine in China's Shendong coalfield, we established a model for overburden movement in the 8.2-m super-high mining face by combining theoretical calculations and numerical simulation. We analyzed the mechanism of incoming pressure and surrounding rock support in the super-high mining face and revealed the spatial and temporal evolution law of roof fracture and crumbling in the far field of the super-high mining face. The research results provide theoretical and technical guidance for the selection of supports and safe and efficient mining of overburden under similar conditions.

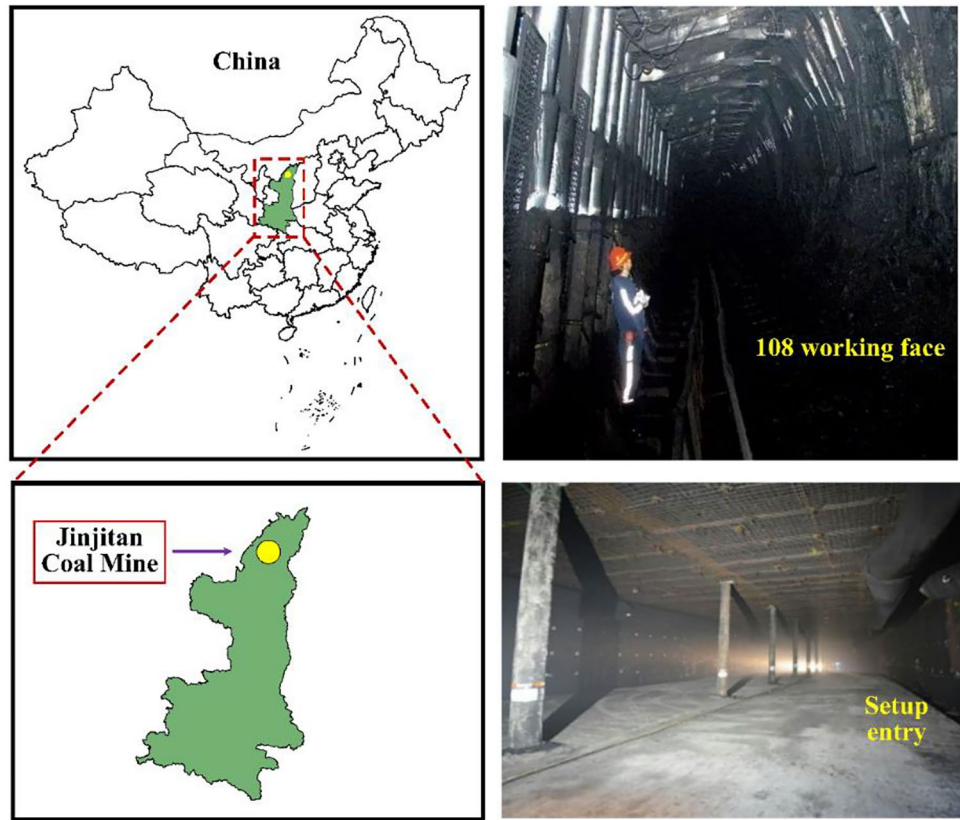## General situation of working face

Project profile

Jinjiitan Coal Mine is located in the northern part of Shaanxi Province, China (Fig. 1), which is part of the transition zone between the Mawuusu Desert and the Loess Plateau; thus, the surface is covered by thick loose weathered sand. The coal mine is mining No. 12 coal seam with an average thickness of 6.65 m and an average mining depth of 246 m. The average thickness of the loose seam is 35 m, which belongs to near shallow seas with an average dip angle of smaller than 1°. The geological conditions in this area are simple, the strata are flat, the overall trend is monoclinic structure, the slope is inclined to the northwest, there is no folding and magmatic activity, and the geological working conditions are suitable for the arrangement of working face with a super-large mining height.

This study is based on the field measurement data of the No. 108 working face, which is the first mining face of the No. 12 coal seam with an average elevation of +97 m. The overall height is high in the east, low in the west, high in the south, and low in the north. The mining slope is 300 m long, and the strike length is 5527 m, and the mining is carried out by one-time full-height coal mining technology. The designed maximum mining height is 8.2 m, and the depth ratio is much smaller than 50. This mining height is the first of its kind in the world.

Mechanics model of stope space structure

The rock formations that need to be controlled in the stope include the determination of the range of collapsed rock formations, the composition of transmitting rock beams, and the height of damaged arches (Wen et al. 2014). The range of collapsed rock strata refers to the "immediate roof" where the old pond has collapsed, and the immediate roof thickness is expressed as follows (Frith and Reed 2018):

Fig. 1 Location of Jinjitan Coal Mine and 108 working face

is the basis for evaluating whether they constitute the same rock beam. The expression is as follows (Yang et al. 2018).

$$M_Z = \sum_{i=1}^{n} M_i = \frac{h - S_A}{K_A - 1} \tag{1}$$

$$S_A = \frac{C_0}{2L_k} \Delta h_0 \tag{2}$$

where N is the number of rock layers that have fallen in the old pond; M_i is the thickness of the fallen rock layers; h is the mining height; K_A is the breaking expansion coefficient of the fallen rock layers; S_A is the settlement value at the place where the rocking beam touches the gangue under the old roof (a constant value smaller than the old roof settlement value S_o); C_0 is the lower rock beam of the old roof which is the first time that the step distance is pressed; L_K is the first time that the top distance is controlled by pressure; and Δh_0 is the first time that the stope roof subsidence is pressured. Among them, the breaking expansion coefficient K_A is determined by the lithological strength of each rock layer existing directly on top. The higher the lithological strength, the greater the value of K_A. Generally, $K_A = 1.25–1.35$.

Through theoretical analysis and studies and comparisons, the deflection inference method was chosen to calculate the transfer rock beam fracture step (Zhao et al. 2018). Whether or not adjacent rock layers move at the same time

$$\begin{cases} \text{Same rock beam } E_S M_S^2 \geq (1.15 \sim 1.25)^4 E_C M_C^2 \\ \text{Different rock beams } E_S M_S^2 < (1.15 \sim 1.25)^4 E_C M_C^2 \end{cases} \tag{3}$$

where M_S is the thickness of the lower strata; E_S is the elastic modulus of the lower strata; M_C is the thickness of the upper strata; and E_C is the elastic modulus of the upper strata.

The compression steps of each transmission rock beam under its weight include the first fracture compression step C_0 and the periodic compression C_i. The steps are respectively given by formulas (4) and (5) (Li et al. 2018).

$$C_0 = \sqrt{\frac{2M_S^2 \sigma_S}{(M_S + M_C)\gamma}} \tag{4}$$

$$C_i = -\frac{1}{2}C_{i-1} + \frac{1}{2}\sqrt{C_{i-1}^2 + \frac{4M_s^2[\sigma_s]}{3\gamma(M_s + M_C)}} \tag{5}$$

where M_S is the thickness of the lower part of the rocking beam (support); M is the thickness of the upper part of the rocking beam; σ_S is the allowable tensile stress of the lower

part (support) of the rock; γ is the average bulk density of the rocking beam; C_i is the current cycle during which the step distance is pressed; and C_{i-1} is the last cycle during which the step distance is pressed (Song et al. 2019), and the simple model is shown in Fig. 2.

When $M_C = 0$ (i.e., when the thickness of the upper part of the rock formation in the above formulas is zero and there is only one rock formation moving at the same time), the rocking beam is composed of a single rock formation (He et al. 2007). The periodic sudden instability of the rock beam changes in the opposite direction of the step distance of the last sudden instability and the bulk density γ_{E1} of the rocking beam, and changes in the positive direction of the thickness M_E and the tensile strength $[\sigma]$ of the rocking beam.

Space movement law of stope

Evolution law of caving zone

When the thickness of the rock layer M_1 is less than the mining height, the rock blocks cannot be arranged regularly after M_1 sinks (Fig. 3). The rock layer group composed of M_1 is called the caving zone. After the overlying rock layer sinks, in the horizontal direction, the horizontal transfer force connection cannot always be maintained between the sinking rock blocks (Huang et al. 2020). When the thickness of the rock layer M_1 is greater than the allowable sinking height, there will be no caving zone. The overhanging stage of the stope roof refers to the working face that is pushed up from the cutoff cut towards the first rock formation with supporting function above the coal seam collapses (i.e., the first collapse step where the advance length (L_x) is smaller than $L_{0(M1)}$ the distance from M_1) (Li et al. 2020a, b).
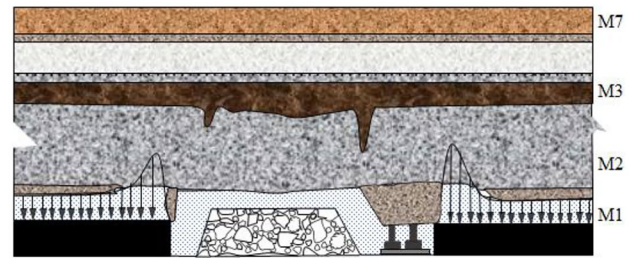

Fig. 3 Formation stage of the caving zone

$$\sigma_{coal} = HL_{0(i)}\gamma / 2S \qquad (6)$$

where σ_{coal} indicates the pressure on the coal wall (kN/m^2;); H represents the buried depth of the coal seam (m); $L_{0(i)}$ denotes the first collapse step of the i-th layer (m); γ stands for the average bulk density of the overlying rock (kN /m^3) (generally $r = 25$ kN/m^3); and S_x signifies support pressure distribution range (m).

After the rock strata in the caving zone collapsed, the horizontal force transmission was lost. The rock layer behind the support fell into the goaf, and its entire weight was supported by the coal floor, while the rock strata in the caving zone above the support (including the suspended roof part) and the weight of the fractured rock layer were all supported by the support. Because the lower rock beam of the fractured rock layer had not experienced the first fracture, the weight of the fractured rock layer had to be transmitted to the coral wall in front of the working face and the coal wall behind the working face through the lower rock beam of the fractured rock layer. σ_{coal} is greater than the uniaxial compressive strength R_{coal} of the coal seam, and the peak of the abutment pressure reaches the front of the coal wall.

Fig. 2 Rock beam fracture mechanics model
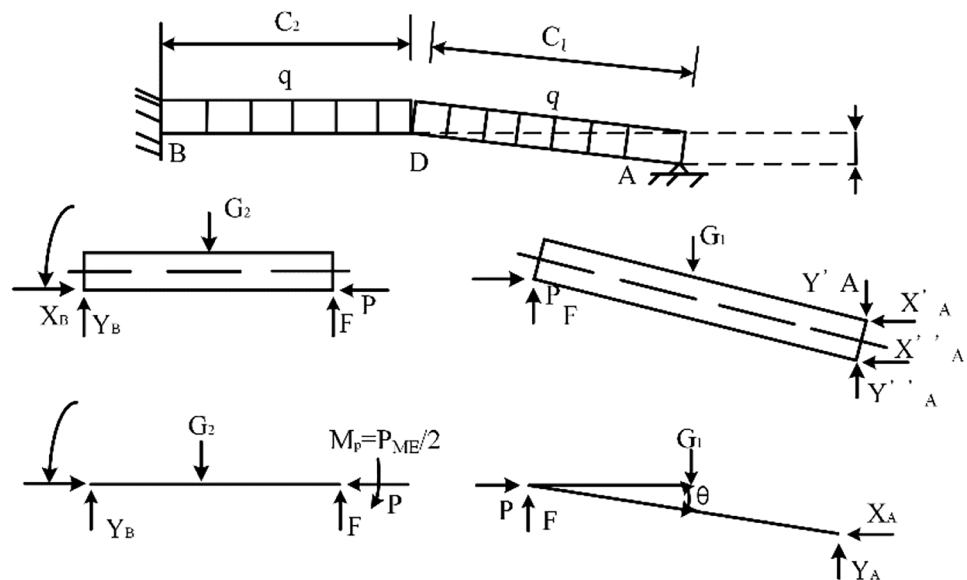
Because the pressure peak shifts to the coal wall, the coal body between the coal wall and the pressure peak is forced to undergo plastic deformation or even failure deformation. On the contrary, there is no plastic zone on the working face if no internal stress appears (Meng et al. 2018).

Movement law of fracture zone

When the coal seam and the caving zone rocks are hard and the buried depth is not enough to cause the coal seam to experience plastic deformation, the lower rock beam fracture of the fractured rock layer is located at the coal wall of the working face (Fig. 4a: point A). In contrast, the fracture of the lower rock beam of the fractured rock layer is located in front of the coal wall of the working face (Fig. 4a: point B). When the coal seam and the lower rock layer are hard, or the upper rock layer has low hardness and the burial depth is not enough to cause the coal seam to undergo plastic deformation, the upper rock beam fracture of the fractured rock layer is located at the coal wall of the working face (Fig. 4b: Point A) (Zhou et al. 2019). On the contrary, the upper rock beam fracture of the fractured rock layer is located in front of the coal wall of the working face (Fig. 4b: point B). At this time, the area of the pressure release zone (i.e., plastic zone) formed between the fracture point and the coal wall increases. This area is called the internal stress field S_0.

The development and change stage of the fractured rock formation starts from the first fracture of the lower rock beam of the fractured rock formation, and the fractured
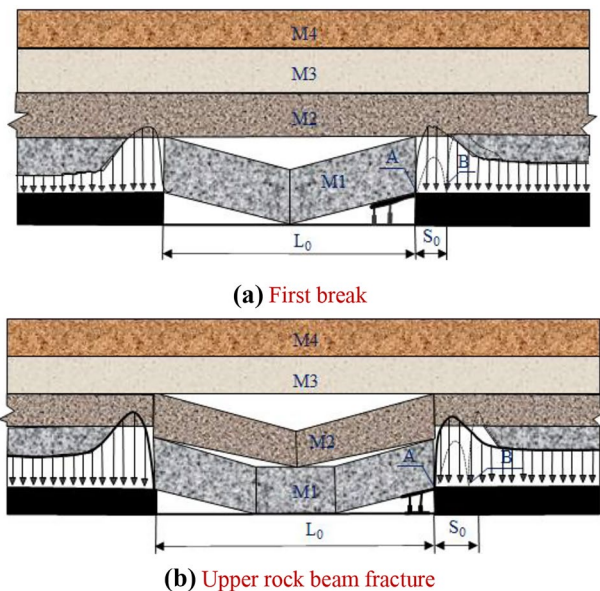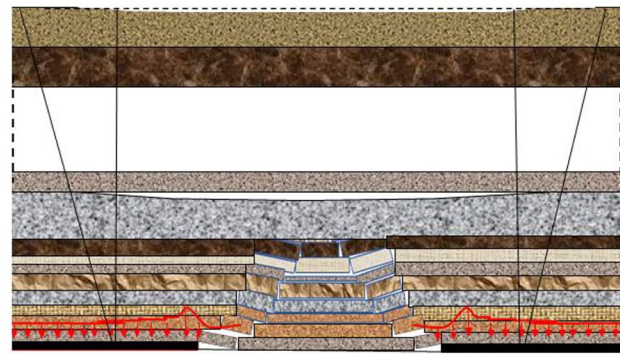

Fig. 5 Development and change stage of the fracture zone

arch is formed when the working face advances towards the inclined length of the working face. The stable stage of fractured rock formation begins when the working face advances towards the inclined length and finishes when the working face advances towards the stop line position (Fig. 5) (Zhu et al. 2022). M_{arch} shows a rocking beam above the stope. When the stope advances to a certain distance (the inclined length of the working face is 300 m), a fractured arch-like linear A is formed in the roof above the stope. At this time, the weight of the rocking beam M_{arch} is supported by the coal bodies on both sides of the stope through the transfer of force between the rock beams; hence, M_{arch} can form a rocking beam that continues to advance in the stope without breaking. When the stope continues to advance, the "damage arch" will only jump forward in the direction of the work front.

Numerical simulation

Model building

The model was built according to the engineering geological conditions of the unmined area of the 108 working face, and horizontal constraints were applied to the front, back, left, and right boundaries of the model, horizontal and vertical
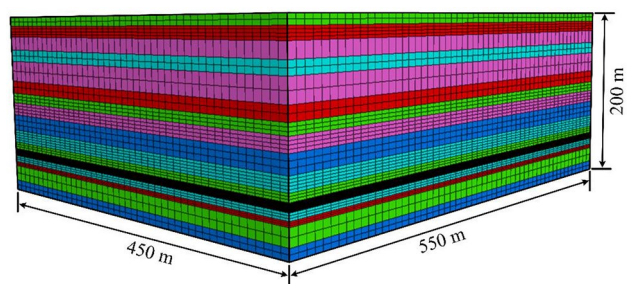

(a) First break

(b) Upper rock beam fracture

Fig. 4 Rock fracture stag

**Fig. 6** Three-dimensional numerical model diagram

Table 1 Physical and mechanical parameters of rock formations

Rock	Density (kg m^{-3})	Elastic modulus (GPa)	Tensile strength (MPa)	Cohesion (MPa)	Poisson ratio	Internal friction angle (°)	Thickness (m)
Fine sandstone	2500	14.64	5.56	4.68	0.22	42	10
Medium sandstone	2350	14.62	5.67	4.27	0.22	34	12
Siltstone	4700	14.59	5.69	4.25	0.21	40	15
Siltstone sandstone interbedding	3600	13.64	5.62	3.97	0.23	41	13
Siltstone	4700	14.59	5.69	4.25	0.21	40	23
Medium sandstone	2350	14.62	5.67	4.27	0.22	34	14
Fine sandstone	2500	14.64	5.56	4.68	0.22	42	11
Siltstone	4700	14.59	5.69	4.25	0.21	40	14
Coarse sandstone	2120	12.37	6.53	3.94	0.23	30.5	18
Siltstone sandstone interbedding	3600	13.64	5.62	3.97	0.23	41	14
Fine sandstone	2500	14.64	5.56	4.68	0.22	42	7.8
Coal	1320	1.92	1.6	0.81	0.26	38	8.2
Siltstone sandstone interbedding	3600	13.64	5.62	3.97	0.23	41	7
Medium sandstone	2350	14.62	5.67	4.27	0.22	34	5
Fine sandstone	2500	14.64	5.56	4.68	0.22	42	17
Coarse sandstone	2120	12.37	6.53	3.94	0.23	30.5	11

constraints were applied to the lower boundary of the model, and equivalent loads in the vertical direction were applied to the upper boundary of the model. $P = \gamma H$ represents the weight of the overlying strata of the model, where γ is the average volumetric force of the overlying strata. The average volume force of the rock formation was 0.023 MN/m^3. H denotes the distance from the upper part of the model to the surface. The calculation grid was divided according to the geometric size of the model, which took into account the limitation of the total number of model units and the concentration of the research problem area. In addition, to prevent the influence of boundary effects on the calculation results (Huang and Zhu 2017; Zhu and Zuang 2017), we increased the front, back, left, and right boundaries of the model by 75 m. The model size is $550 \times 450 \times 200$ m. The specific model shape is shown in Fig. 6, and the Cullen Moore model is used. The model is divided into 7 layers from the bottom up, which are Coarse Sandstone, Fine Sandstone, Medium Sandstone, Siltstone Sandstone Interbedding, Coal, Fine Sandstone, Siltstone Sandstone Interbedding,

Fig. 7 Distribution of the plastic zone at different distances from the working face to the cutoff: **a** 96 m; **b** 102 m; **c** 123 m; **d** 126 m
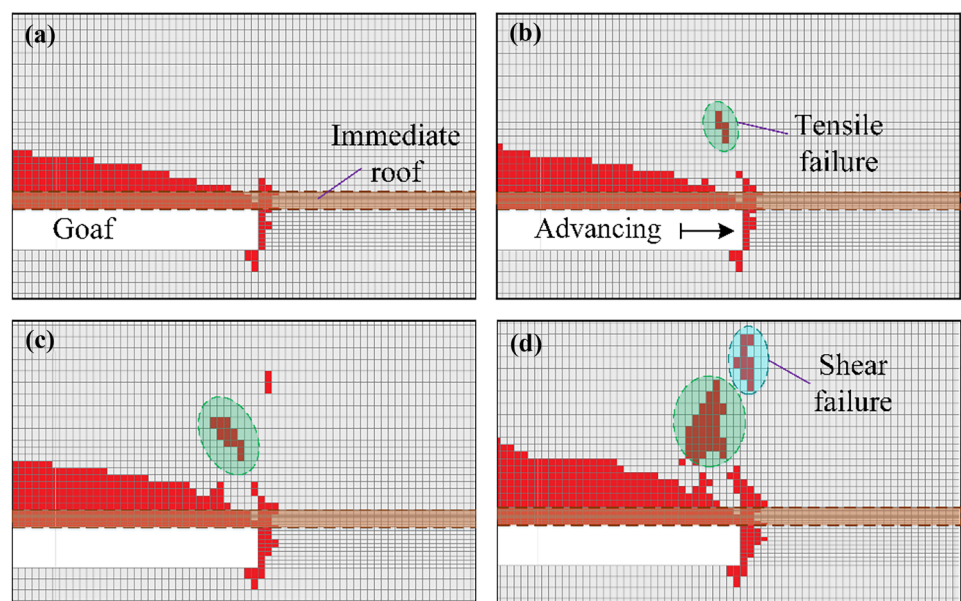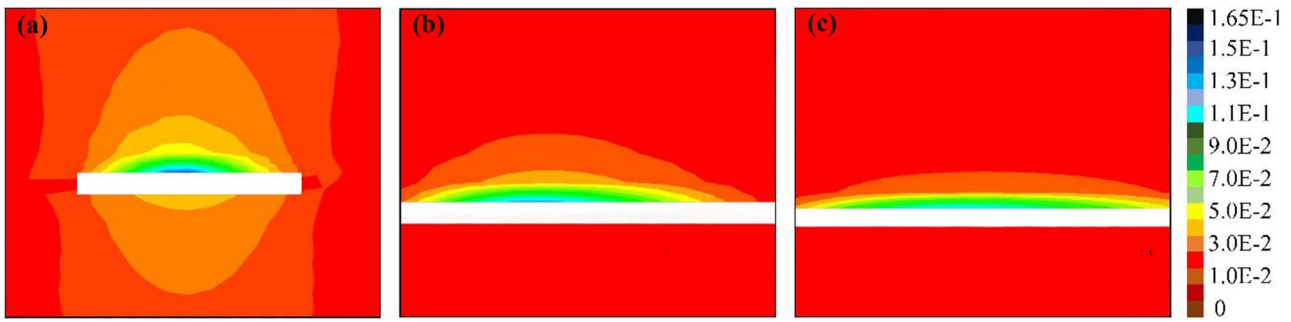
Fig. 8 Variation in overburden deformation as the working face advances **a** 80 m; **b** 160 m; **c** 300 m

Coarse Sandstone, Siltstone, Fine Sandstone, Medium Sandstone, Siltstone, Siltstone Sandstone Interbedding, Siltstone, Medium Sandstone and Fine Sandstone, and the mechanical parameters of each rock layer and coal seam in the top and bottom plates are shown in Table 1.

Numerical simulation results

With the advancement of the working face, the area of the goaf, the overhang span of the overburden, and the plastic failure range of the overburden of the goaf also expanded. Figure 7a shows that when the working face advanced to 96 m away from the open-off cut, the immediate roof collapsed in a small area, while the old roof was likely in an overhanging state without large-scale plastic failure. Figure 7b indicates that when the working face advanced to 102 m of the open-off cut, the immediate roof continued to collapse, and tensile failure areas appeared on both sides of the old roof near the upper end of the support. The tensile stress received at this time exceeded the maximum tensile strength; thus, the old roof broke at both ends, and the damage tended to extend to the coal walls on both sides. After the initial pressure was applied to the old roof of the working face, along with the continuous advancement of the working face, the structure formed by the old roof would change based on the pattern of "stability-instability-stability." Fig. 7c displays that when the working face advanced to

123 m away from the open-off cut, the overhanging space of the old roof continued to increase and the old roof cracked, rotated, and sank under the action of its gravity. Figure 7d reveals that the old roof had a large shear failure area near the upper part of the two ends of the support, and a large range of tensile failure areas appeared in the middle and lower parts of the old roof, forming a periodic compression, and the compression step was about 24 m.

The movement and deformation of the overlying rock under the different propelling positions of coal mine working face or mining heights in coal mines were different, and the height of the resulting overlying rock fissure zone was also different. The displacement of the overlying strata and the height of the fracture zone at different distances from the cut hole are shown in Figs. 8, 9 and Table 2. The calculation results demonstrated that because the front and back sides of the mining space were supported by rock masses, for the rock strata near the roof of the mined-out area, the overburden at the same buried depth produced the largest deformation in the middle of the span. Besides, the movement of this deformation towards both sides gradually decreased, and the vertical direction of the upper rock strata in the goaf was symmetrical. When the working face advanced to 80 m away from the open-off cut, the maximum deformation near the center of the roof was 0.17 m, while the deformation near the open-off cut was within 0.05 m and the gradient changes were obvious. It can be observed from the map of overburden displacement and the height of

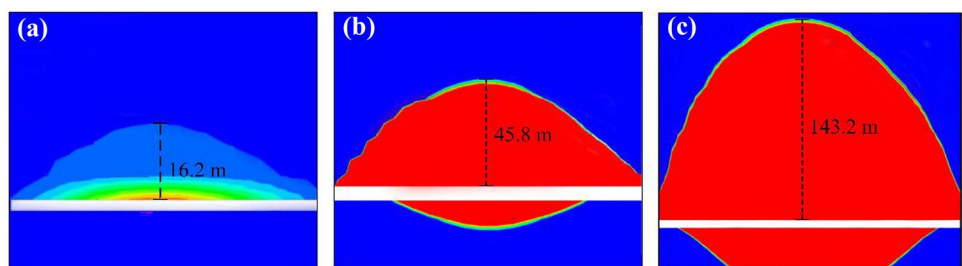**Fig. 9** Variation in fracture height as the working face advances **a** 80 m; **b** 160 m; **c** 300 m

Table 2 Deformation and crack height under different excavation lengths

Sort	Excavation length (m)	Maximum deformation (m)	Fissure height (m)
(a)	80	0.17	16.2
(b)	160	1.27	45.8
(c)	300	5.80	143.2

the fracture zone that the working face advanced to 160 m away from the cut hole, the maximum deformation was 1.27 m, and the fracture height was 45.8 m. In the stratum located 20 m above the roof (with deformations smaller than 0.1 m) and the surface, the rock mass deformations were very small. Therefore, the vertical displacement of the overburden was the largest. As the overburden gradually approached the surface, the displacement of the rock gradually decreased. The rock formation collapse in the goaf was mainly concentrated on the top of the rock layer and its vicinity. Near the surface, the impact of the goaf on the rock formation collapse was small.

The law of mining pressure at a large mining height

The characteristics of the first pressure

According to the field measurement and research analysis regarding the working face with a large mining height in the near shallow buried coal seam, due to the large increase in the thickness of the one-time mining, the original immediate roof (geological immediate roof) is far from being able to fill the goaf, and the old roof of the original lower group collapses. When it falls behind, it cannot form a hinge structure and it is falling, which is equivalent to direct top action. Based on the structural characteristics of the overlying strata in the working face with a large mining height, the hard roof

of the near shallow buried coal seam is manually cut at the end to form a cantilever beam. According to the equivalent theory of gravity acceleration generated by the synthesis of external forces, the immediate roof of the working face with a large mining height should be redefined as: between the coal seam and the hinged old roof rock layer. The caving zone rock layer that cannot form a structure is called the equivalent immediate roof (Fig. 10). Note that the original part of the old roof and the original immediate roof that fall in the goaf together form the caving height.

Based on the direct full roof of the mined-out area and considering the break-up coefficients of different equivalent immediate roofs, the maximum thickness of the equivalent immediate roof can be calculated as follows (Wang et al. 2022):

$$\sum h = \frac{M}{K_p - 1} = 3.5M \tag{7}$$

where $\sum h$ is the equivalent immediate roof thickness (m); M is the mining height (m); and K_p is the breaking expansion coefficient of the equivalent immediate roof. According to the relevant research, the mining height above 6 m K_p can generally be 1.3–1.35, and the calculated equivalent immediate roof thickness is about 3 to 3.5 times the mining height.

The equivalent immediate roof of the near-shallow buried face with a large mining height is shown as a double-key layer structure such that the lower group of key layers is a step beam structure and the upper group of key layers is a "short masonry beam" structure. When the height increases and the equivalent immediate roof becomes thicker, the hinged structure of the key layer under the roof moves up, forming a double-group structure model for the roof of the working face with a large mining height (Fig. 11). The "masonry beam" structure is formed by the upper group of key layers, and the lower group of key layers form a step beam structure with a thick equivalent directly roof on top form a double-key layer structure together. Due to the existence of two groups of structures in the working face with a large mining height,

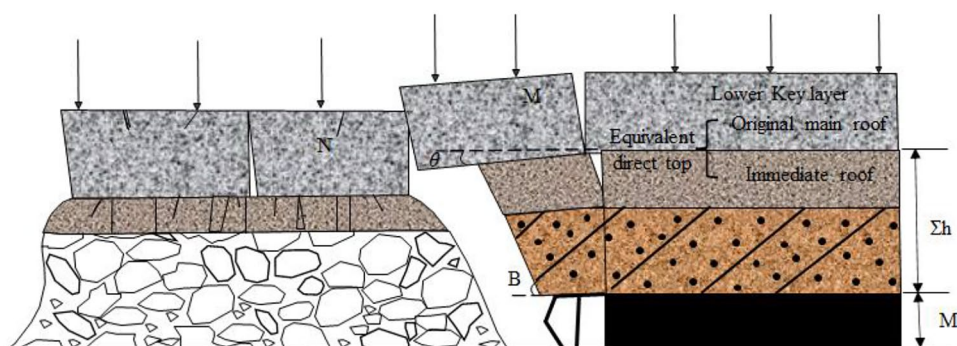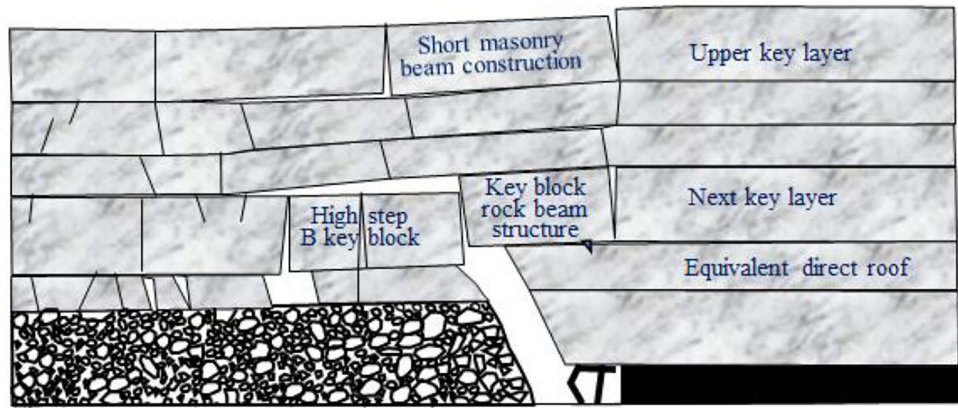**Fig. 10** Diagram of equivalent direct roof structure model with a large mining height

Fig. 11 Double-group structure model of the roof in the working face with a large mining height


the working face will have large and small periodic pressure. The movement of the high-level stepped rock beam structure of the lower-key layer results in a small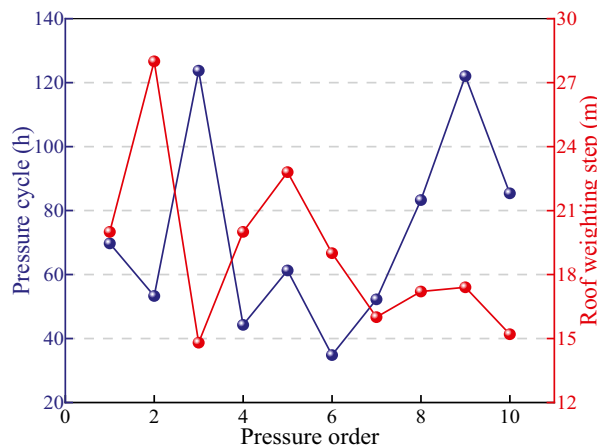 period of compression. Furthermore, the short masonry beam structure of the upper key layer and the lower stepped rock beam structure overlap to form a large period of compression. Generally, the step distance is about twice as long as that of the small cycle.
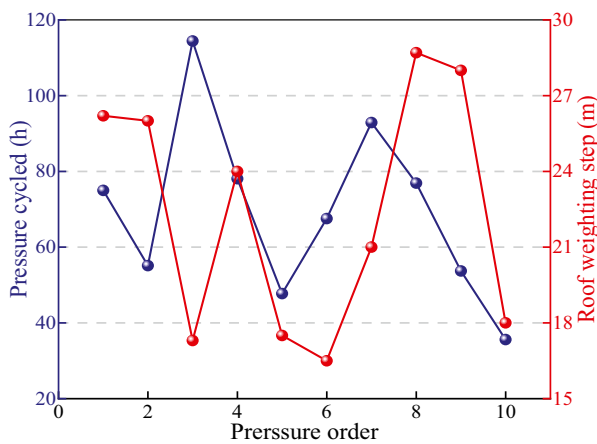
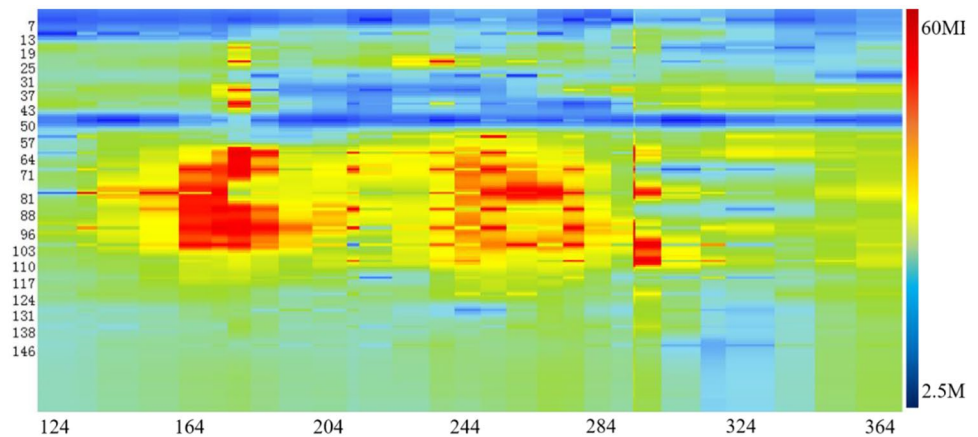**(a)** Upper station monitoring data
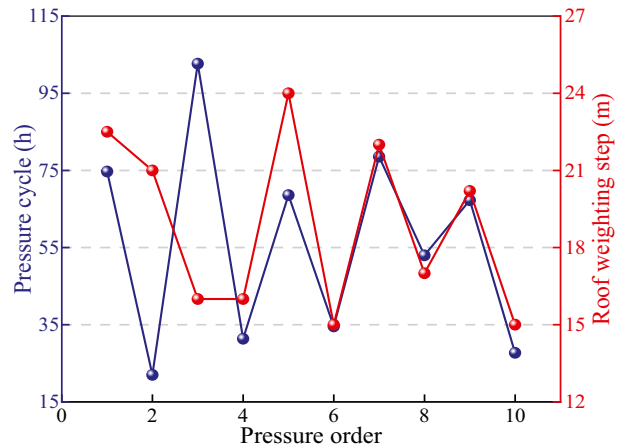
(b) Central station monitoring data

(c) Lower station monitoring data

Fig. 12 Periodic pressure time and pressure step of the No. 108 working face

Fig. 13 Comprehensive stress distribution diagram of the No. 108 working face

The characteristics of the periodic pressure

Online fully mechanized support manometers were installed in the middle of the working face support, slide head, and slide tail. Through real-time monitoring data analysis on the site, we found that the No. 108 working face had 12 cycles of pressure from the end of the initial pressure till the advancement of the working face to 375 m. The overall pressure in the middle of the working face was large, and the pressure at the two ends was small (Fig. 12 for the periodic pressure time and step distance). The old top fractures of the No. 108 working face showed the large and small periodic pressure and step distance, and the step distance of the large periodic pressure was about 28.7 m, and that of the small periodic pressure was about 15 m.

It can be observed from the comprehensive stress distribution of the working face (Fig. 13) that the stress in the middle of the working face was large. The pressure value of the No. 60–No. 103 supports in the range of 164–194 m was between 44 and 46 MPa; the pressure value of the No. 60–No. 103 brackets in the range of 234–254 m was about 41 MPa; the pressure value of the No. 60–No. 110 brackets in the range of 234–254 m was about 40–46 MPa; and the pressure of the upper and lower ends was small.

The influence of mining speed on periodic pressure

To study the influence of the advancement speed of the working face on the law of incoming pressure, three stages with obvious differences in the advancement speed were chosen for the whole mining practice of the No. 108 working face for the sake of comparison as follows: fast advancement (11.2 m/d), normal advancement (9.6 m/d), and slow speed advancement (5.6 m/d). Table 3 shows the statistics of working face pressure parameters corresponding to the above three stages. To accurately determine the periodic pressure law at different advancement speeds, 24 measuring stations were installed to detect pressure data on the No. 108 working face, and the whole working face was evenly distributed according to the upper, middle, and lower three measuring areas. The 24-h average curve that reflects the basic top-period pressure rule in the three stations is shown in Fig. 14, and the characteristics of the pressure period at different propulsion speeds are shown in Table 2. When the working face was advancing slowly, the dynamic load coefficient was small, and the periodic pressing step and the duration of the pressing were shorter. Moreover, when the working face was advancing rapidly, the dynamic load coefficient was larger, and the periodic weighting step increases. The distance and the incoming pressure lasted longer. Compared with slower propulsion, during fast propulsion, the step length and continuous length of incoming pressure increased significantly (increased by 65.8% and 138.5%, respectively). The load of the support increased by 2.8% during the loading period, and the load of the support decreased during the non-compression period by 13%. When accelerating the advancement of the working face based on slow

Table 3 comparison of cycles with different advancement speeds in the No. 108 working face

Group	Mining speed (m/d)	Mining height (m)	Pressureless support load (MPa)	Pressure support load (MPa)	Periodic weighting step (m)	Mining length in pressure (m)
A	11.2	7–7.5	20.24	47.6	32	4.5–5.4
B	9.6	6.65	22.05	47.6	27.6	3.7–4.6
C	5.6	6	23.90	43.4	19.3	3.6–3.9

(a) 5.6 m/d of propulsion

(b) 9.6 m/d of propulsion
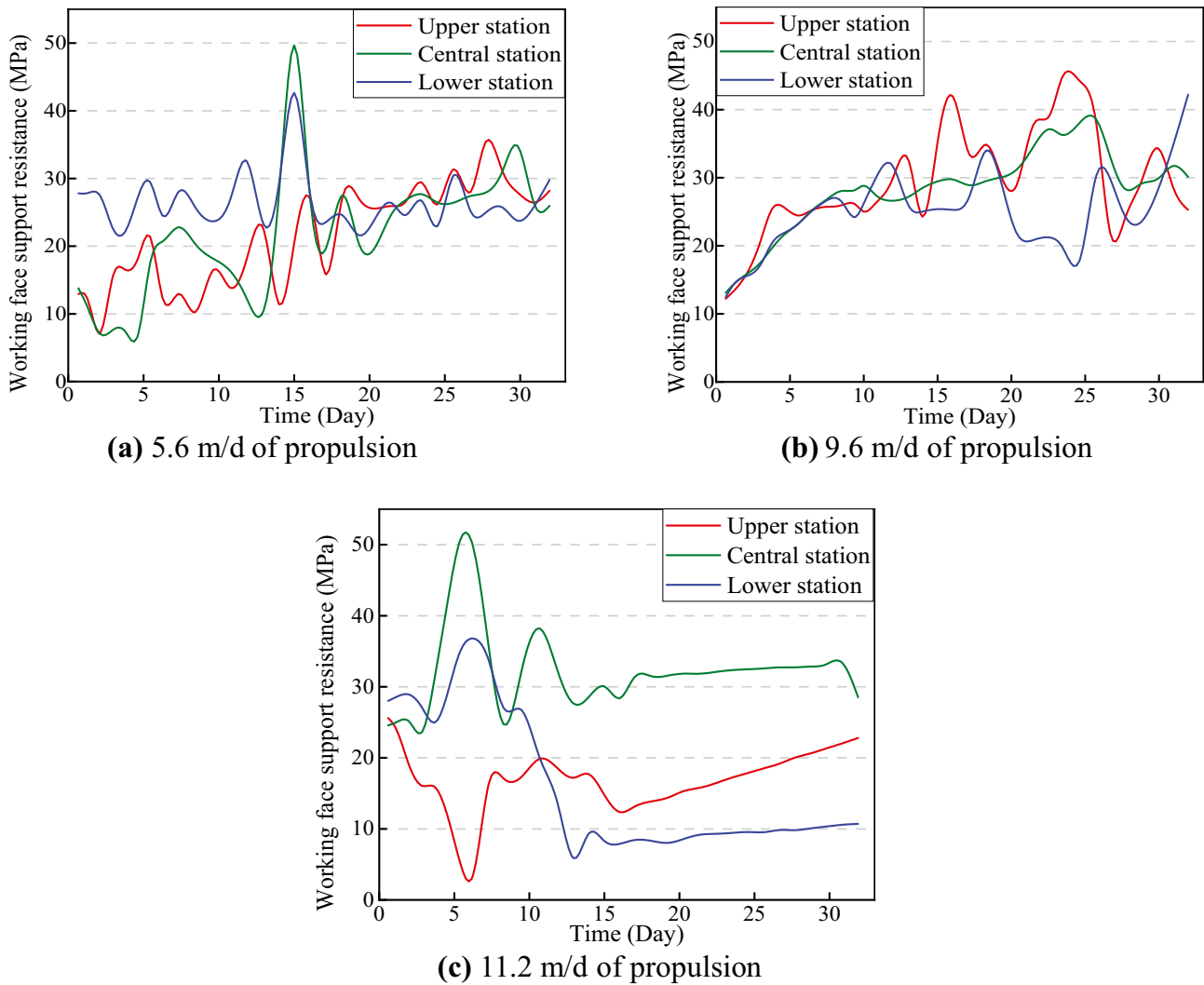
(c) 11.2 m/d of propulsion

Fig. 14 24-h average pressure at different advanced speeds on the working face

advancement, the roof weighting step and the continuous length of the pressure increased significantly, and when the advancement speed of the working face reached a certain level (for example, an increase from 9.6 m/d to 11.2 m/d), compression step distance and other parameters did not change much and only the continuous length of the compression increased by 17.4%.

Conclusion

We investigated the problem of rock seam pressure variation in oversized mining faces in near-shallow buried coal seams. The three-dimensional numerical model was solved by theoretical analysis and FLAC^{3D}, and the characteristics of rock pressure appearance and surrounding rock control countermeasures in a fully mechanized coal mining face

with a super high mining height of 8.2 m were analyzed by combining the actual measured data at the working face. The main conclusions were as follows:

1. A rock beam fracture mechanics model was established. The deflection inference method was selected to calculate the transmission rock beam fracture distance and to analyze the formation stage of the caving zone, the rock fracture stage, the development and change stage of the fracture zone, and the mining subsidence model. The evolution law of the falling zone, the movement law of the fracture zone, and the evolution law of the subsidence moving zone were obtained accordingly.

2. The equivalent immediate roof structure model and the double group structure model of the large mining height roof were obtained through the analysis of engineering measured data in the near shallow buried coal seam.

Besides, the influence of the characteristics of the periodic incoming pressure and the speed of recovery on the periodic incoming pressure were acquired.

3. The initial pressure step of the old roof of the working face was 102 m. With the continuous advancement of the working face, the structure formed by the old roof would undergo a change based on the pattern of "stability-instability-re-stability," and the periodic pressing step of the old roof was about 24 m. Near the roof, the vertical displacement of the overlying rock layer was the largest. As the overlying rock layer gradually approached the surface, the displacement of the rock layer gradually decreased. The working face was moved to 300 m, the maximum deformation of the rock mass was 5.8 m, and the crack height was 143.2 m.

4. The advancement speed of the No. 108 working face was slow during the initial mining period, and the high roof pressure promoted the thickening of the equivalent immediate roof of the caving zone. Through field observation of the old roof when there was no incoming pressure, the support pressure was maintained between 23 and 26 MPa, the empty roof distance from the goaf was smaller than 4 m, the cutoff roof braking effect was ideal, and the immediate roof collapsed with the mining. This delayed the key rock beam of the old roof pressure step for the first fracture. The pressure was small during the non-compression period.

Declarations

References

Bai EH, Guo WB, Tan Y (2019) Negative externalities of high-intensity mining and disaster prevention technology in China. B Eng Geol Environ 7(87):5219–5235

Chen SJ, Zhang JC, Yin DW, Cheng XZ, Jiang N (2022) Relative permeability measurement of coal microchannels using advanced microchip technology. Fuel 312:122633

Cheng T, Tang G, Liu C, Wang H (2017) A zoning model for coal mining-induced strata movement based on microseismic monitoring. Int J Rock Mech Min 94(3):123–138

Frith R, Reed G (2018) Coal pillar design when considered a reinforcement problem rather than a suspension problem. Int J Min Sci Techno 28(1):11–19

Guo GC, Yang YK (2021) The study of key stratum location and characteristics on the mining of extremely thick coal seam under goaf. Adv Civ Eng 2021:8833822

Hao XG, Song M, Feng Y, Zhang W (2017) De-capacity policy effect on China's coal industry. Energies 12(12):2331

He MC, Zhang GF, Qi G, Li Q, Jia QZ, Zhou J (2007) Stability control of surrounding rocks in deep entry of Jiahe coal mine. J Min Saf Eng 24(1):27–31 (in Chinese)

He X, Zhao YX, Yang K, Zhang C, Han PH (2021) Development and formation of ground fissures induced by an ultra large mining height longwall panel in Shendong mining area. B Eng Geol Environ 80(10):7879–7898

Huang QX, Zhou JL, Cao J (2020) Key stratum structure and support working resistance of longwall face with large mining height in the shallow coal seams. China Adv Civ Eng 2020:8834403

Huang Y, Zhu CQ (2017) Safety assessment of antiliquefaction performance of a constructed reservoir embankment. I: Experimental assessment. J Perform Constr Fac 31(2):04016101

Le TD, Mitra R, Oh J, Hebblewhite B (2017) A review of cavability evaluation in longwall top coal caving. Int J Min Sci Techno 27(6):907–915

Li B, Liang YP, Zou QL (2019a) Determination of working resistance based on movement type of the first subordinate key stratum in a fully mechanized face with large mining height. Energy Sci Eng 7(3):777–798

Li H, Zhang DS, Jiang SY, Fan GW, Xu MT (2019b) Mechanism of secondary breakage in the overlying strata during repetitious mining of an ultrathick coal seam in design stage. Adv Civ Eng 2019:5090326

Li M, Zhang JX, Huang YL, Gao R (2017) Measurement and numerical analysis of influence of key stratum breakage on mine pressure in top-coal caving face with super great mining height. J Cent South Univ 24(8):1881–1888

Li XL, Cao ZY, Xu YL (2020a) Characteristics and trends of coal mine safety development. Energ Source Part A 2020:1–14

Li XL, Chen SJ, Liu SM, Li ZH (2021a) AE waveform characteristics of rock mass under uniaxial loading based on Hilbert-Huang transform. J Cent South Univ 28(6):1843–1856

Li XL, Chen SJ, Zhang QM, Gao X, Feng F (2021b) Research on theory, simulation and measurement of stress behavior under regenerated roof condition. Geomech Eng 26(1):49–61

Li Z, Xu Jl JuJF, Zhu WB, Xu JM (2018) The effects of the rotational speed of voussoir beam structures formed by key strata on the ground pressure of stopes. Int J Rock Mech Min 108:67–79

Li ZH, Pang YK, Bao YS, Ma ZY (2020b) Research on surface failure law of working faces in large mining height and shallow buried coal seam. Adv Civ Eng 2020:8844249

Liu H, Deng KZ, Zhu XJ, Jiang CL (2019) Effects of mining speed on the developmental features of mining-induced ground fissures. B Eng Geol Environ 78(8):6297–6309

Lu CJ, Xu JP, Zhao H, Zhang H, Zhang YA, Chen MY (2022) Floor disturbance and failure characteristics of super-large mining height working face. Geofluids 2022:1279642

Meng ZS, Zeng QL, Gao KD, Kong S, Liu P, Wan LR (2018) Failure analysis of super-large mining height powered support. Eng Fail Anal 92:378–391

Shi XC, Zhang JX (2021) Characteristics of overburden failure and fracture evolution in shallow buried working face with large mining height. Sustainability 13(24):13775

Song ZQ, Hao J, SHI YK, Tang JQ, Liu JK (2019) An overview of connotation and development of practical ground pressure contorl theory. J Shandong Univ Sci Techno 38(1):1–15 (in Chinese)

Unver B, Yasitli N (2006) Modelling of strata movement with a special reference to caving mechanism in thick seam coal mining. Int J Coal Geol 66(4):227–252

Wang S, Li XL, Qin QZ (2022) Study on surrounding rock control and support stability of ultra-large height mining face. Energies 15(18):6811

Wen Z, Xing E, Shi S (2019) Overlying strata structural modeling and support applicability analysis for large mining-height stopes. J Loss Prevent Proc 57:94–100

Wen ZJ, Qu GL, Wen JH, Shi YK, Jia CY (2014) Deformation failure characteristics of coal body and mining induced stress evolution law. Sci World J 2014:714507

Wu FF, Liu CY, Yang JX (2016) Mode of overlying rock roofing structure in large mining height coal face and analysis of support resistance. J Cent South Univ 23:3262–3272

Wu SL, Li YC, Chen YQ, Li L (2020) Analysis and evaluation of support performance of multi-service support in Gaotouyao coal mine. J Shandong Univ Sci Techno 39(03):50–58 (in Chinese)

Yan H, Zhang JX, Feng RM, Wang W, Lan YW, Xu ZJ (2020) Surrounding rock failure analysis of retreating roadways and the control technique for extra-thick coal seams under fully-mechanized top caving and intensive mining conditions: a case study. Tunn Undergr Sp Tech 97:103241

Yang Z, Liu C, Tang SC (2018) Rock burst mechanism analysis in an advanced segment of gob-side entry under different dip angles of the seam and prevention technology. Int J Min Sci Techno 28(6):55–63

Yu B, Zhao J, Kuang TJ, Meng XB (2015) In situ investigations into overburden failures of a super-thick coal seam for longwall top coal caving. Int J Rock Mech Min 78:155–162

Yuan Y, Tu SH, Zhang XG, Bo Li (2013) System dynamics model of the support-surrounding rock system in fully mechanized mining with large mining height face and its application. Int J Min Sci Techno 23:879–884

Zhao Y, Wang S, Zou Z, Fang C (2018) Instability characteristics of the cracked roof rock beam under shallow mining conditions. Int J Min Sci Techno 28(3):437–444

Zhou DW, Wu K, Bai ZH, Hu ZQ, Li L, Xu YK, Diao XP (2019) Formation and development mechanism of ground crack caused by coal mining: effects of overlying key strata. B Eng Geol Environ 78(2):1025–1044

Zhu CL, Zhang JX, Li M, He ZW, Wang YY, Lan YW (2022) Effect mechanism of strata breakage evolution on stope deformation in extra-thick coal seams. Alex Eng J 61(6):5003–5020

Zhu CQ, Zuang Y (2017) Safety assessment of antiliquefaction performance of a constructed reservoir embankment. II: Numerical assessment. J Perform Constr Fac 31(2):04016102

Zhu SY, Jiang ZQ, Zhou KJ, Peng GQ, Yang CW (2014) The characteristics of deformation and failure of coal seam floor due to mining in Xinmi coal field in China. B Eng Geol Environ 73(4):1151–1163